BeBeC-2020-S06

ADAPTIVE PROJECTION BEAMFORMING

Robert P. Dougherty[1]
[1]OptiNav, Inc.
1414 127th PL NE #106, 98004, Bellevue, WA, USA

ABSTRACT

Engineering results from a microphone phased array should ideally include component spectra reflecting the sound radiated from Regions of Interest within the field of view. A new processing method for producing component spectra, Functional Projection Beamforming, was introduced in 2019. It offers high dynamic range and consistent integration of coherent as well as incoherent source distributions. Functional Projection Beamforming falls short in resolution, limiting its usefulness at low frequency. Another new method, Adaptive Projection Beamforming is presented here. It has been obtained by combining the ideas of adaptive beamforming and projection beamforming, giving the benefits of both. It can operate with just a few grid points, instead of the complete map needed for deconvolution processing. Adaptive Projection Beamforming performs significantly better than the Functional version at low frequency and compares well with other advanced techniques on Array Methods Experimental Benchmark datasets DLR-1 and NASA 2.

1 INTRODUCTION

Consider a microphone phased array and a corresponding beamform map. The beamform map is a color contour plot that contains a number of peaks that may represent the locations of acoustic sources. For example, in a common case, the array is used to image a wing that produces noise at the leading and trailing edges. The beamform map includes apparent line sources are the edges. The quantities of interest are the spectra from the two edges, either total or per unit length, to the exclusion of the effects of the other edge and interfering noise from the lateral edges and unwanted noise source in the wind tunnel. A Region of Interest, ROI, is defined that contains a portion of the trailing edge, for example. The problem is to process the array data so as to give the spectra associated with the ROI. An obvious method is to compute a conventional beamforming map using Frequency Domain Beamforming, FDBF, integrate over the ROI, and normalize by the integral over a model point source compensate for peak spreading. This has three problems. The resolution is limited because the ROI may include part of a peak from a source outside the ROI. The dynamic range is limited because a

threshold must be set high enough to avoid integrating sidelobes. Finally, the basis of the integration approach is an assumption that various sources within the ROI are mutually incoherent so that their beamforming powers add. This last problem is may be important in trailing noise, for example, because the turbulence implicated in its creation has a nonzero coherence length in the spanwise direction. An alternative method, Deconvolution processing, can be slow and becomes confusing for coherent sources.

Functional Projection Beamforming, FPB, [1,2] extends the idea of Functional Beamforming [3-5] to grids of coherent or incoherent or sources within an ROI. It gives the speed and dynamic range of Functional Beamforming while correctly accounting for the multiple sources whether they are coherent or not. Its resolution is no better than conventional beamforming. The Adaptive Projection Beamforming, APB, method presented here resolves the resolution problem of FPB. In addition, methods for addressing a high-frequency limitation of FPB/APB have been developed and are also described. The APB formula and its derivation are given below, followed by several examples at Technology Readiness Levels 4 and 5.

2 DERIVATION AND FORMULAS

Suppose the microphone array has N transducers and the ROI contains M grid points. Each grid point has a steering vector of length N. Arranging these on the columns of an $N \times M$ matrix gives $\boldsymbol{G} = [\boldsymbol{g}_1, \dots, \boldsymbol{g}_M]$. Following the derivation in [1] and [2], the array Cross Spectral Matrix, CSM, has the model

$$\boldsymbol{C} = \mathrm{E}[(\boldsymbol{G}\boldsymbol{q})(\boldsymbol{G}\boldsymbol{q})'] + \boldsymbol{N} = \boldsymbol{G}\boldsymbol{S}\boldsymbol{G}' + \boldsymbol{N} \tag{1}$$

where $\boldsymbol{q}$ is the narrowband time history of the sources, $\boldsymbol{S}$ is the source cross spectral matrix to be characterized, and $\boldsymbol{N}$ is interference from sources outside the ROI. Using the Singular Value Decomposition, SVD of $\boldsymbol{G}$, the model is re-written

$$\boldsymbol{C} = \boldsymbol{U}_1 \boldsymbol{W} \boldsymbol{U}_1' + \boldsymbol{N} \tag{2}$$

where $\boldsymbol{U}_1$ is an $N \times n_1$ matrix consisting of the first n_1 left singular vectors of $\boldsymbol{G}$, and,$n_1$is the number of significant singular values. The problem in analyzing Eq. (2) is to find the best matrix $\boldsymbol{W}$ for a given, measured, $\boldsymbol{C}$. If a least-squares fit is taken as the measure of "best", then the solution is the Projection Beamforming formula, $\boldsymbol{W}_{\mathrm{PB}} = \boldsymbol{U}_1{}' \boldsymbol{C} \boldsymbol{U}_1$. The dynamic range can be improved by replacing this with the FPB formula $\boldsymbol{C}_{\mathrm{FPB}} = \left[\boldsymbol{U}_1 \boldsymbol{U}_1{}' \boldsymbol{C}^{\frac{1}{\nu}} \boldsymbol{U}_1 \boldsymbol{U}_1{}'\right]^{\boldsymbol{\nu}} = \boldsymbol{U}_1 \left[\boldsymbol{U}_1' \boldsymbol{C}^{\frac{1}{\nu}} \boldsymbol{U}_1\right]^{\nu} \boldsymbol{U}_1{}'$ where $\nu \geq 1$.

Experience with FPB has shown that, in the case of a large ROI at high frequency, it can happen that $n_1 = N$, removing all resolution from the method. This can be avoided by choosing a subset of $M_1 < N$ steering vectors from the M steering vectors in the ROI, and forming $\boldsymbol{G}$ from these. In the software considered here, these are chosen to maximally non-parallel in an iterative process. Let a distance between steering vectors be defined as the reciprocal of the magnitude of the inner product of the normalized steering vectors. The first two steering vectors in the set are the pair associated with the ROI with largest relative distance. The next steering vector to be added is the one from the ROI that has not been used yet and maximizes the minimum distance to the steering vectors already in the set. Steering vectors are added according to this criterion until the given number, M_1, are found.

The PB and FPB formulas are not optimal in terms of resolution because neither $\boldsymbol{C} - \boldsymbol{U}_1\boldsymbol{W}_{\mathrm{PB}}\boldsymbol{U}_1{}'$ nor $\boldsymbol{C} - \boldsymbol{C}_{\mathrm{FPB}}$ are guaranteed to be positive semidefinite. In contrast, adding this restriction to $\boldsymbol{C} - \boldsymbol{U}_1\boldsymbol{W}_{\mathrm{proposed}}\boldsymbol{U}_1'$ increases the resolution of the method because it decreases the set of allowed $\boldsymbol{W}$ results, excluding those that are not fully compatible with $\boldsymbol{C}$ and $\boldsymbol{U}_1$.
Suppose the problem is defined to mean "find the largest $\boldsymbol{W}$ such that $\boldsymbol{C} - \boldsymbol{U}_1\boldsymbol{W}\boldsymbol{U}_1{}'$ is positive semi-definite." The meaning of "largest" in this case is that adding any positive Hermitian matrix to $\boldsymbol{W}$ would cause the sum to no longer pass the test.

In the SVD of $\boldsymbol{G}$, let $\boldsymbol{U} = [\boldsymbol{U}_1\boldsymbol{U}_2]$, where $\boldsymbol{U}_1 = \left[\boldsymbol{u}_1, \dots, \boldsymbol{u}_{n_1}\right]$, as before, and $\boldsymbol{U}_2 = \left[\boldsymbol{u}_{n_1+1}, \dots, \boldsymbol{u}_N\right]$. The inequality to be optimized by $\boldsymbol{W}$ is

$$\boldsymbol{C} - \boldsymbol{U}_1\boldsymbol{W}\boldsymbol{U}_1{}' \geq \boldsymbol{0} \tag{3}$$

A change of basis is performed by multiplying on the left by $\boldsymbol{U}'$and the right by $\boldsymbol{U}$, giving

$$\boldsymbol{U}'\boldsymbol{C}\boldsymbol{U} - \boldsymbol{U}'\boldsymbol{U}_1\boldsymbol{W}\boldsymbol{U}_1'\boldsymbol{U} \geq \boldsymbol{0} \tag{4}$$

Introduce the notation $\boldsymbol{D}_{ij} = \boldsymbol{U}_i{}'\boldsymbol{C}\boldsymbol{U}_j$, $i,j = 1,2$. Let the test vector to evaluate whether Eq. (4) is true or not be denoted

$$\boldsymbol{x} = \begin{bmatrix}\boldsymbol{x}_1\\ \boldsymbol{x}_2\end{bmatrix}$$

where $\boldsymbol{x}_1$ is an n_1-vector and $\boldsymbol{x}_2$ is an n_2-vector, $n_2 = N - n_1$. In the new basis, inequality (3) and (4) becomes

$$\boldsymbol{x}_1'(\boldsymbol{D}_{11} - \boldsymbol{W})\boldsymbol{x}_1 + \boldsymbol{x}_1'\boldsymbol{D}_{12}\boldsymbol{x}_2 + \boldsymbol{x}_2'\boldsymbol{D}_{21}\boldsymbol{x}_1 + \boldsymbol{x}_2'\boldsymbol{D}_{22}\boldsymbol{x}_2 \geq 0 \quad \forall\, \boldsymbol{x}_1, \boldsymbol{x}_2 \tag{5}$$

Given an $\boldsymbol{x}_1$, the worst-case $\boldsymbol{x}_2$ would be found by minimizing the LHS of Inequality (5) wrt. $\boldsymbol{x}_2$. But this a quadratic function of the elements of $\boldsymbol{x}_2$ and can be minimized explicitly by $\boldsymbol{x}_2 = -\boldsymbol{D}_{22}^{-1}\boldsymbol{D}_{21}\boldsymbol{x}_1$. Substituting this back into In. (5) gives

$$\boldsymbol{x}_1'(\boldsymbol{D}_{11} - \boldsymbol{D}_{21}'\boldsymbol{D}_{22}^{-1}\boldsymbol{D}_{21} - \boldsymbol{W})\boldsymbol{x}_1 \geq 0 \quad \forall\, \boldsymbol{x}_1 \tag{6}$$

This has an unambiguous solution: $\boldsymbol{W} = \boldsymbol{D}_{11} - \boldsymbol{D}_{21}'\boldsymbol{D}_{22}^{-1}\boldsymbol{D}_{21}$. Adding any matrix with a positive eigenvalue to $\boldsymbol{D}_{11} - \boldsymbol{D}_{21}'\boldsymbol{D}_{22}^{-1}\boldsymbol{D}_{21}$ and substituting the sum for $\boldsymbol{W}$ into Inequality (6) would produce a contradiction if the eigenvector were used for $\boldsymbol{x}_1$.
In terms of the original variables

$$\boldsymbol{W}_{\mathrm{APB}} = \boldsymbol{U}_1{}'\boldsymbol{C}\boldsymbol{U}_1 - \boldsymbol{U}_1{}'\boldsymbol{C}\boldsymbol{U}_2(\boldsymbol{U}_2{}'\boldsymbol{C}\boldsymbol{U}_2)^{-1}\boldsymbol{U}_2{}'\boldsymbol{C}\boldsymbol{U}_1 \tag{7}$$

The first term in the APB formula is recognized as $\boldsymbol{W}_{\mathrm{PB}}$ and the second term is a correction for high resolution. This equation is theoretically interesting and works well on synthetic data if a small regularization diagonal is added inside the parentheses. In the case of real microphone array data, it has been found that the regularization parameter has to be so large that FPB outperforms it.

As an aside, it should be noted that this formulation reduces to standard adaptive beamforming, or the Capon method, for $M = 1$.

In order to produce a stable version of APB, the CSM is first rewritten $\boldsymbol{C} = \boldsymbol{C}^{\frac{1}{2}}\boldsymbol{C}^{\frac{1}{2}}$. Let $\boldsymbol{U}_2 = \left[\boldsymbol{u}_{n_1+1}, \dots, \boldsymbol{u}_N\right]$ and define $\boldsymbol{P}_1 = \boldsymbol{U}_1{}'\boldsymbol{C}^{\frac{1}{2}}$. and $\boldsymbol{P}_2 = \boldsymbol{U}_2{}'\boldsymbol{C}^{\frac{1}{2}}$, .Eq. (7) becomes

$$\boldsymbol{W}_{\mathrm{APB}} = \boldsymbol{P}_1\boldsymbol{P}_1{}' - \boldsymbol{P}_1\boldsymbol{P}_2{}'(\boldsymbol{P}_2\boldsymbol{P}_2{}')^{+}\boldsymbol{P}_2\boldsymbol{P}_1{}' \tag{8}$$

where the Moore-Penrose inverse $(\quad)^+$ is called out explicitly.
Letting the SVD of $\boldsymbol{P}_2$ be written $\boldsymbol{P}_2 = \overline{\boldsymbol{U}}\,\overline{\boldsymbol{\Sigma}}\,\overline{\boldsymbol{V}}'$, the projected CSM becomes

$$\boldsymbol{U}_1\boldsymbol{W}_{\mathrm{APB}}\boldsymbol{U}_1{}' = \boldsymbol{U}_1\boldsymbol{U}_1{}'\left[\boldsymbol{C} - \boldsymbol{C}^{\frac{1}{2}}\overline{\boldsymbol{V}}\boldsymbol{\Gamma}\,\overline{\boldsymbol{V}}'\boldsymbol{C}^{\frac{1}{2}}\right]\boldsymbol{U}_1\boldsymbol{U}_1{}' \tag{9}$$

Here $\boldsymbol{\Gamma}$ is a diagonal matrix with a total of N values, the first m of which are ones and the others are all 0. The range of m is $0 \le m \le n_2 = N - n_1$. The value m controls the resolution and the stability of the method. In the maximum resolution version, $m = n_2$. At the other extreme, $m = 0$, the method reduces to PB. The matrix in brackets can be understood to be a version of $\boldsymbol{C}$ that has been adjusted to improve the resolution.

In the examples below, a diagonal element $\boldsymbol{\Gamma}$ was chosen to be 1 if the corresponding singular value of $\boldsymbol{P}_2$ divided by $\sqrt{\mathrm{tr}(\boldsymbol{C})}$ was greater than a certain threshold, μ. Otherwise, that diagonal element $\boldsymbol{\Gamma}$ was taken as 0. After $\boldsymbol{C}$ was updated by subtracting $\boldsymbol{C}^{\frac{1}{2}}\overline{\boldsymbol{V}}\boldsymbol{\Gamma}\,\overline{\boldsymbol{V}}'\boldsymbol{C}^{\frac{1}{2}}$, the new CSM was used in Functional Projection Beamforming. In other words, the final projected CSM is

$$\boldsymbol{C}_{\mathrm{APB}} = \boldsymbol{U}_1\left[\boldsymbol{U}_1{}'\left(\boldsymbol{C} - \boldsymbol{C}^{\frac{1}{2}}\overline{\boldsymbol{V}}\boldsymbol{\Gamma}\,\overline{\boldsymbol{V}}'\boldsymbol{C}^{\frac{1}{2}}\right)^{\frac{1}{\nu}}\boldsymbol{U}_1\right]^{\nu}\boldsymbol{U}_1{}' \tag{10}$$

2.1 Controlling the method

The APB method, in its current form, has three adjustable parameters: M_1, μ, and ν. These need to be tuned on a case-by-case basis to optimize the results. The beamforming is very fast, so experimentation is quick.

Values of μ in the range of 0.06 to 0.3 have been found to be optimal in the tests to date. Reducing μ increases m in Eqs. (9) and (10), improving the resolution at low frequency. This makes the measured values of weak sources smaller, closer to their true values. However, if μ is too small, then strong sources in a given ROI can suddenly disappear, since they have been incorrectly classified as interference.

The value of ν controls the dynamic range. Optimal values have been found in the range of 10 to 200. Increasing ν increases the dynamic range, but making it too large can make the spectral level too low at high frequency. It appears that FPB and APB are less sensitive to large values of ν than Functional Beamforming is.

The choice of M_1 is typically close to $N/2$. In one case, it has been found best to set it equal to N and let n_1 be controlled to be less than N by a 99% energy criterion for selecting significant singular values in the SVD of $\boldsymbol{G}$.

One issue to bear in mind is that grid points corresponding to the selected steering vectors should not be farther apart than the spot size of the array. If the spot is too small, then sources could fall in between. This criterion limits the size of the ROI because the number of steering vectors is constrained by N. The difficulty can be reduced by shading the array at high frequency to increase the spot size. In the example, binary shading is applied: microphones that are too far from the center of the array are excluded.

3 EXAMPLES

Three measured examples are given below to illustrate the performance of the method. Synthetic examples are not shown because they understate the importance of measurement errors.

3.1 Warehouse test

A test using a miter saw and a loudspeaker driven with broadband noise is shown in Fig. 1. The two noise sources are positioned on a concrete floor to create extended sources between the direct and reflected propagation. The array is a SIG ACAM 100 with 40 microphones, supported by some other hardware that is unrelated to this test. The distance from the array to the sources is 2 m. The horn tweeter inside the loudspeaker is burned out, so all of the radiation from this unit is created by the midrange cone, given a very extended, complex, source at high frequency.

Figure 2 shows conventional beamforming with only the loudspeaker operating at 2368 Hz. Since the 10 dB down point of the peak coincides with the saw location at this frequency, it graphically illustrates that the Rayleigh frequency limit for separating the sources is 2368 Hz.

The ROIs for the saw and speaker processing are shown in Fig. 3. A Quantitative Beamforming plot for 8471 Hz is also shown. The ROIs are designed to be large enough to include the direct and reflected paths from each source, but it is not necessary for them to enclose the whole beamforming peak at low frequency. The locations of some of the source points for the M_1 steering vectors are also indicated as magenta spots. The array has $N = 40$ microphones, and all of them were used at all frequencies. The parameters for the APB processing to follow are $M_1 = 40$, $\mu = 0.3$, and $\nu = 20$.

Spectra for the individual sources are shown in Fig. 4. For frequencies below 4565 Hz, the loudspeaker was the dominant source, so the main beamforming challenge is to reconstruct the saw spectrum in the presence of the interference from the loudspeaker. Above 4565 Hz, the two sources are comparable in level with one or another higher at any given frequency depending primarily on the interference between the direct and reflected paths for the loudspeaker.

Spectral results are shown in Figs. 5-7. In each case, the beamforming curves represent the integrals from one of the regions of interest for data that was recorded with both sources operating. In each plot, a curve representing the array median spectrum with only the source in the selected ROI operating is also shown. This is the exact result that the beamforming integral is attempting to reproduce.

Figure 5 shows the spectra from the saw ROI produced with conventional beamforming integration. For frequencies below the Rayleigh limit of 2368 Hz, the orange curve from the integration is well above the blue curve for the saw-alone data. The difficult actually begins at higher frequency, 4 kHz, where the speaker is 14.6 dB above the saw as shown in Fig. 4. At high frequency, above 7 kHz, the integrated result is also 1-2 dB too high. The only portion of the spectrum where the conventional integration matches the exact result very well is in between, 4-7 kHz.

Figure 6 considers the saw ROI with FBF and APB. Both methods give excellent agreement with the exact result for frequencies above 4 kHz. Like conventional integration, FPB has difficulty below 4 kHz, but the error is smaller, especially for frequencies between the Rayleigh limit and 4 kHz. Adaptive Projection Beamforming stays close to the correct result down to 1269 Hz, about half of the Rayleigh frequency. This is a common observation for superresolution beamforming results; they typically can improve on the Rayleigh limit, or the Sparrow limit, by a factor of 2 [6]. At 1269 Hz, where APB is still operating correctly, the speaker is 21.24 dB louder than the saw. In the next bin down in frequency, the APB result jumps about 20 dB up to match the FPB result. This occurred because the threshold $\mu = 0.3$

was not met for any singular value of $\boldsymbol{P}_2$, at this frequency, giving $m = 0$. The jumps in the APB spectrum at lower frequency reflect an effect of the choice of the threshold value.

FPB and APB Results for the speaker ROI are shown in Fig. 7. The FPB and APB curves match the speaker-alone spectrum well, except in the nulls of the interference between the direct and reflected speaker source. Conventional beamforming integration, not shown, gave very similar results. The coherent source distribution did not cause problems for any method in this case. Presumably a near field array would be more sensitive to coherence effects.

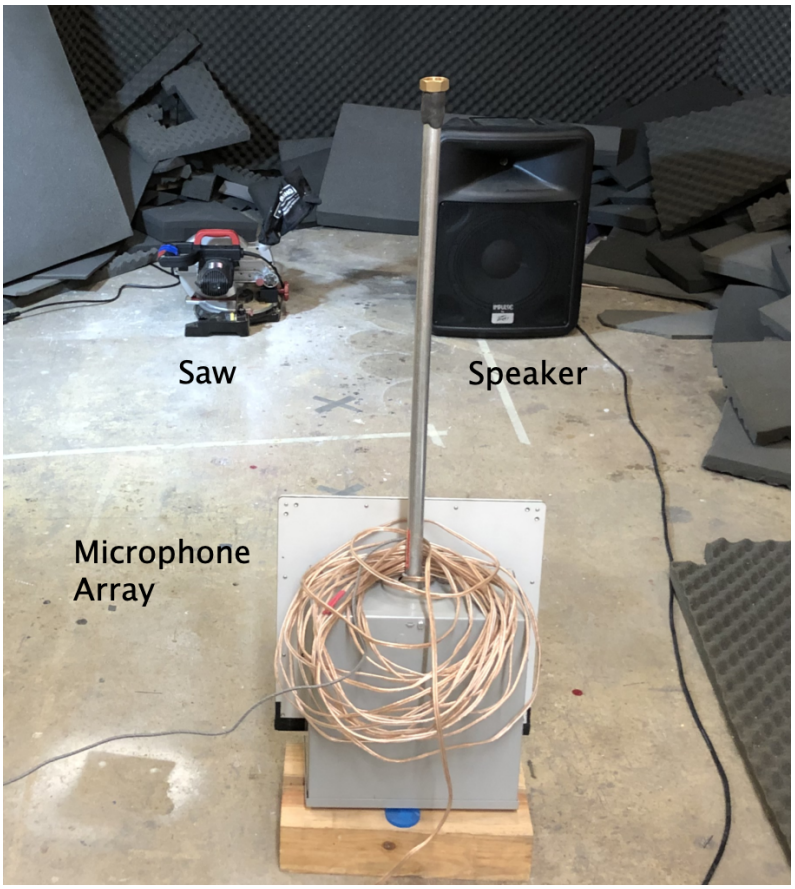

Fig. 1 Setup for a warehouse test.

Fig.2 Illustration of the Rayleigh limit frequency limit for the warehouse test.

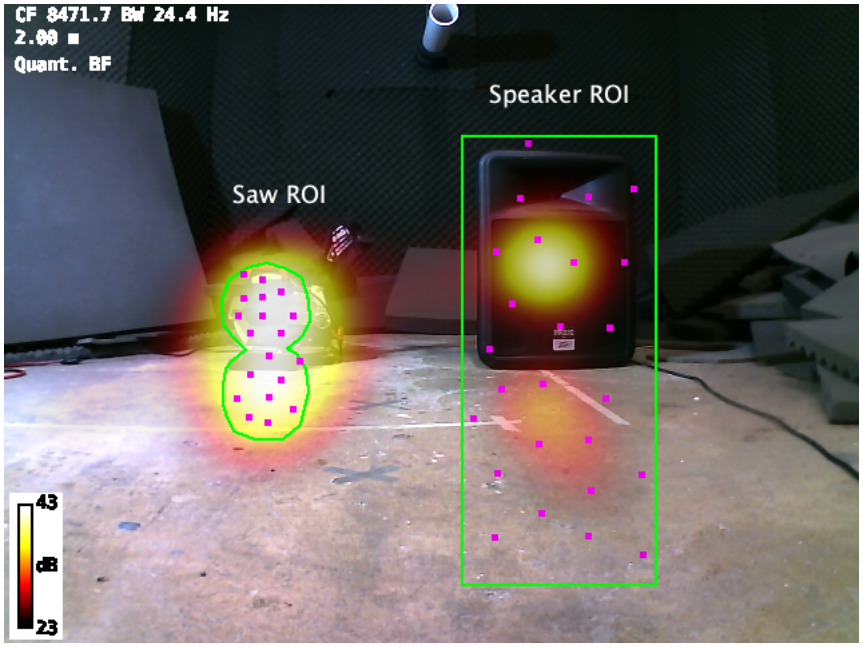

Fig. 3 Regions of Interest for the warehouse test. Some of the grid points for the selected steering vectors are also shown. The FPB/APB computation actually had 40 points in each ROI.

Fig. 4 Array median spectra for the individual sources.

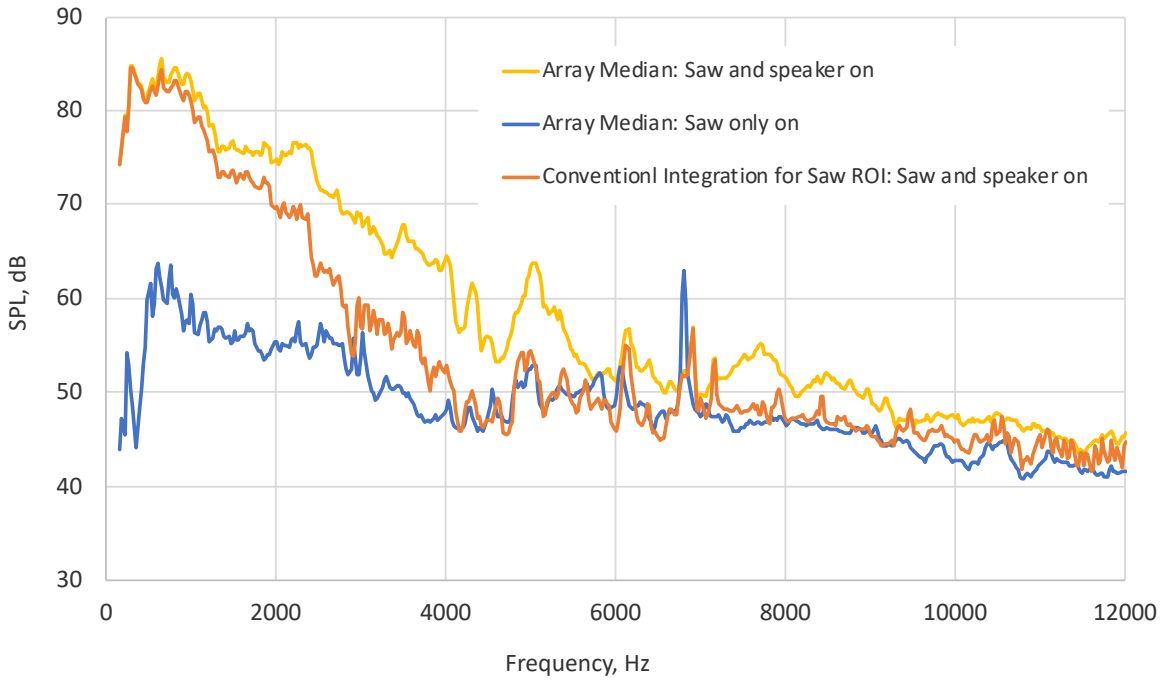

Fig. 5 Spectra from conventional beamforming integration for the Saw ROI.

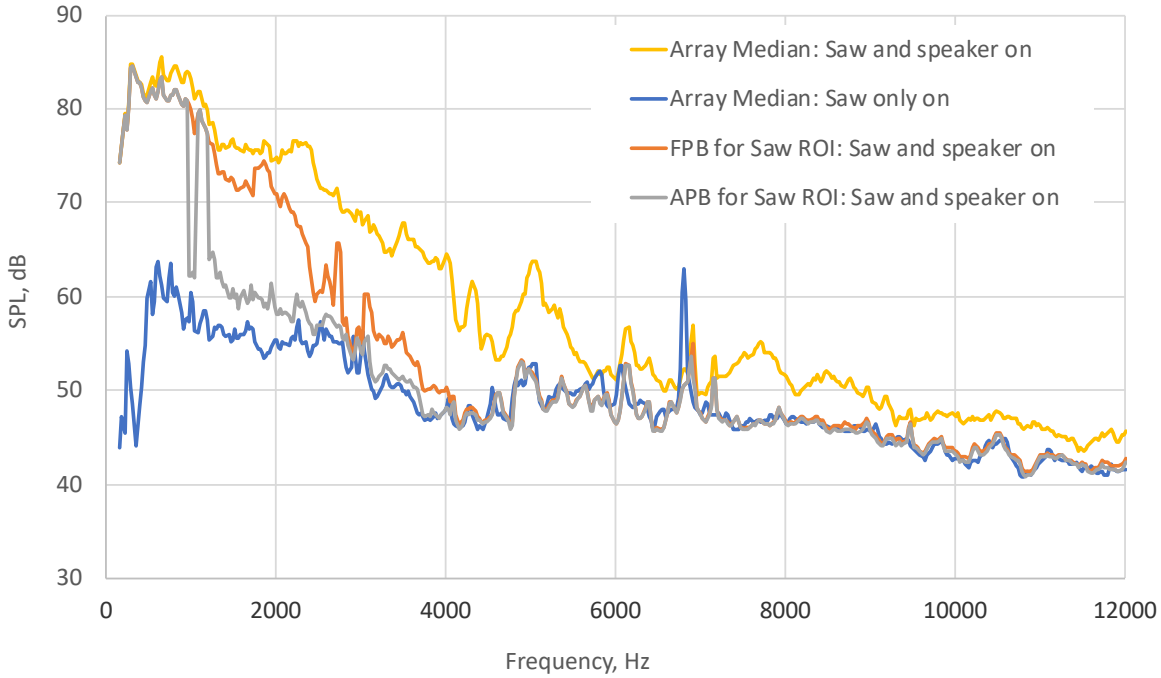

Fig. 6 Spectra from FPB and APB for the Saw ROI.

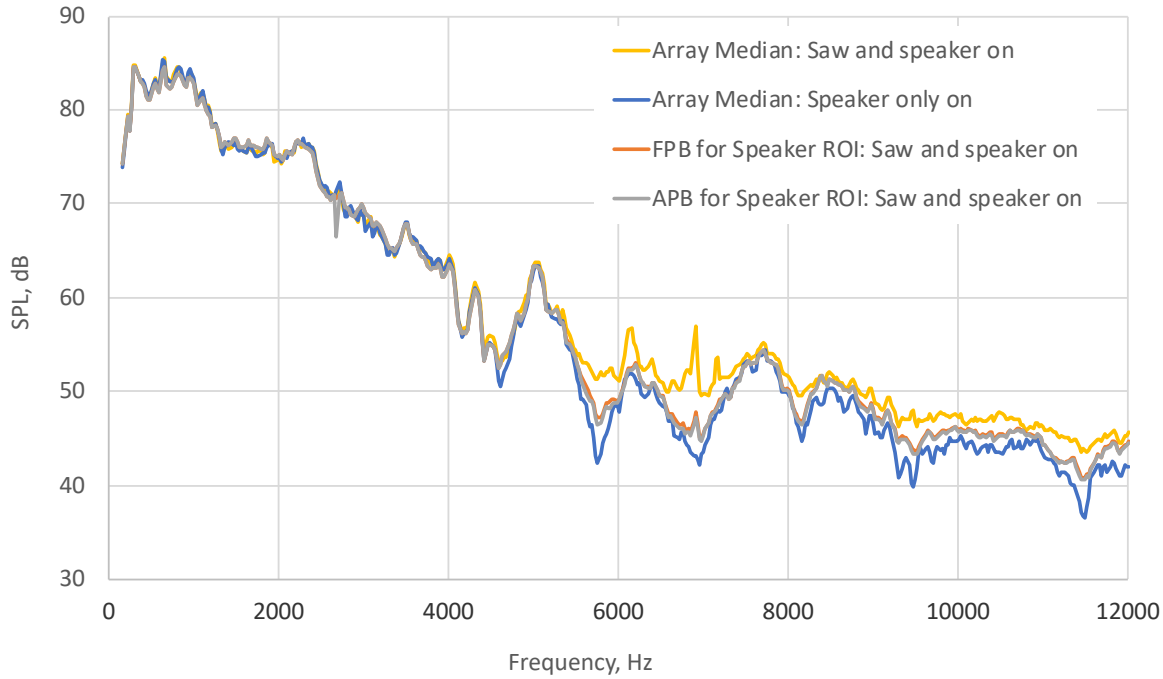

Fig. 7 Spectra from FPB and APB for the Speaker ROI.

3.2 DLR 1

Array Methods Experimental Benchmark dataset DLR 1 is a Donrnier-728 semi span model tested in the high lift configuration in the DLR-Cologne site [7]. The experimental data for the following results were downloaded from the Benchmark data repository [8]. The test setup in shown in Fig. 8.

One-third octave band FB images are shown in Fig. 9. These were produced by summing results from 1/12th OB FB maps. Apart from the outboard leading edge, the dominant sources are the inboard Krueger flap on the inboard leading edge, the outboard flap edge, and the flap track fairings. The ROIs for selected components are shown in Fig. 10. An additional ROI for background noise is included.

The array data from the benchmark files had 135 microphones. The case analyzed was run 59, which an angle of attack of 3° and a Mach number of 0.25. A dead microphone, channel 41, was removed, leaving 134. Binary array shading was applied with the goal of excluding outer microphones for frequencies of 20 kHz and above, where the cutoff radius scaled in proportion to the reciprocal of the frequency. The minimum number of microphones after shading was 65. The APB parameters for the analysis were $M_1 = 20$, $\mu = 0.2$, and $\nu = 20$. The grid spacing was 0.01 m.

Results for narrowband APB for the outboard flap edge are shown in Fig. 11. Results for CLEAN-SC taken from the Benchmark data repository (0.01 m grid) from DLR are also shown. Figure 11 should be compared with the Fig. 6 in Ref. 8.

One twelfth octave band results for the components using conventional beamforming integration and APB are shown in Figs. 12 and 13, respectively. The spread between the levels is much higher with APB. For example, at 10 kHz, the flap edge noise is about 24 dB above the background component using APB, but only 14 dB with conventional integration.

The component plot for FPB is not shown because it is almost identical to Fig. 13 for APB. The adaptive correction did not play a significant role in processing the DLR 1 data.

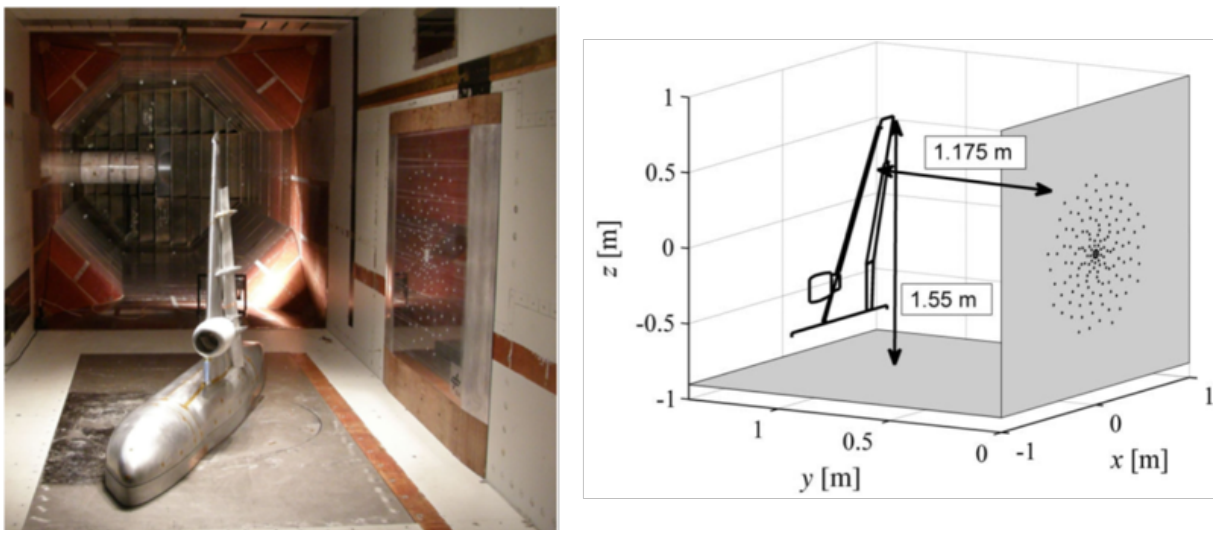

Fig. 8 Setup for Benchmark DLR-1, from Refs. 7 and 8.

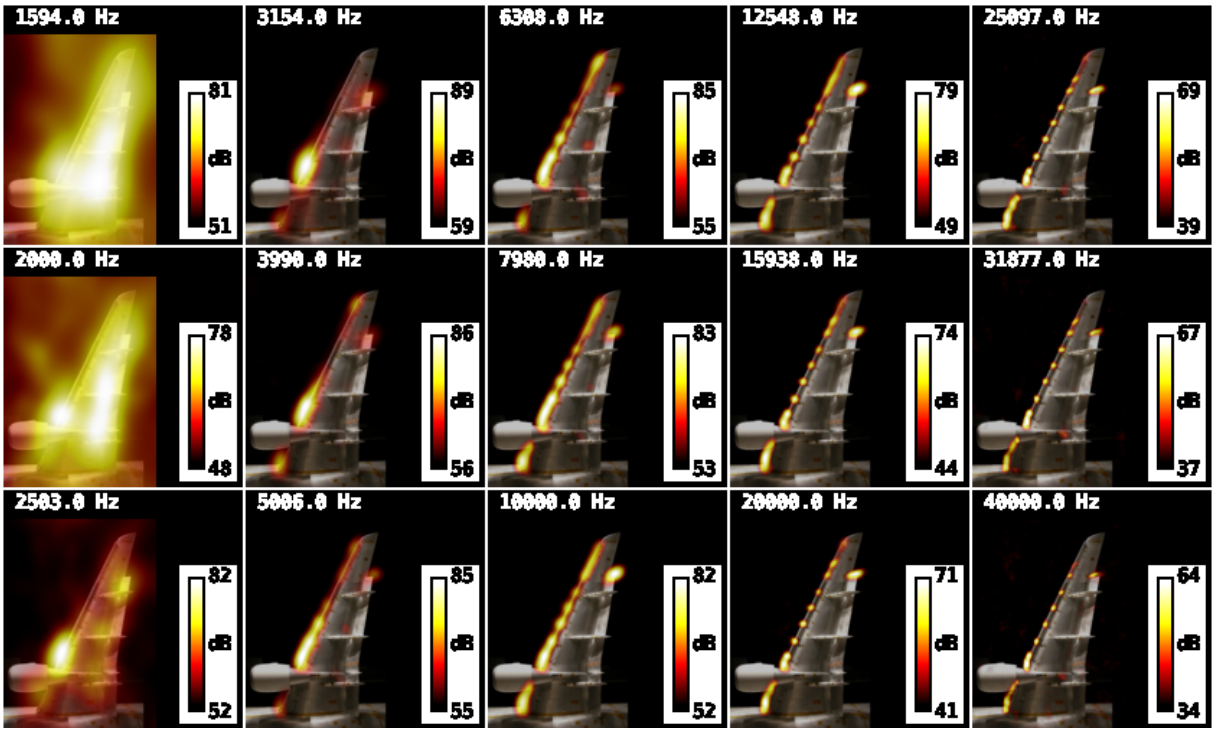

Fig.9 Functional Beamforming with ν = 200 for DLR 1

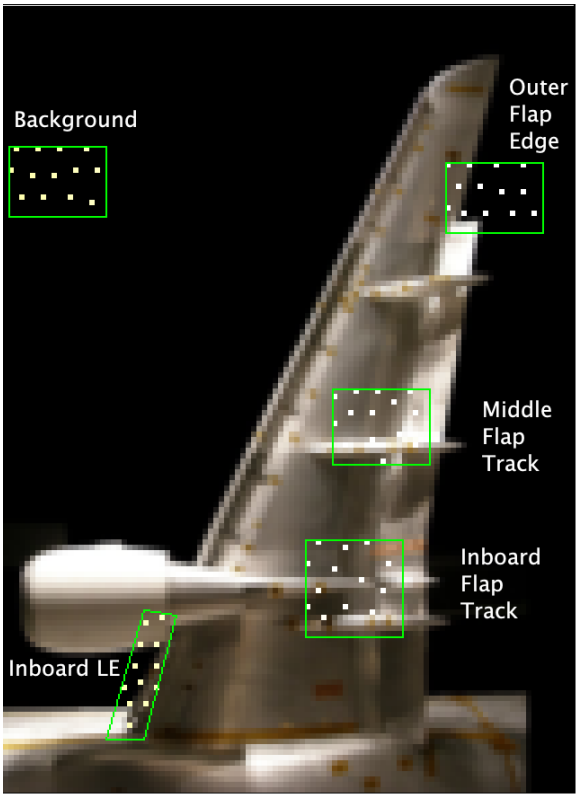

Fig. 10 ROIs and source point grids for DLR=1.

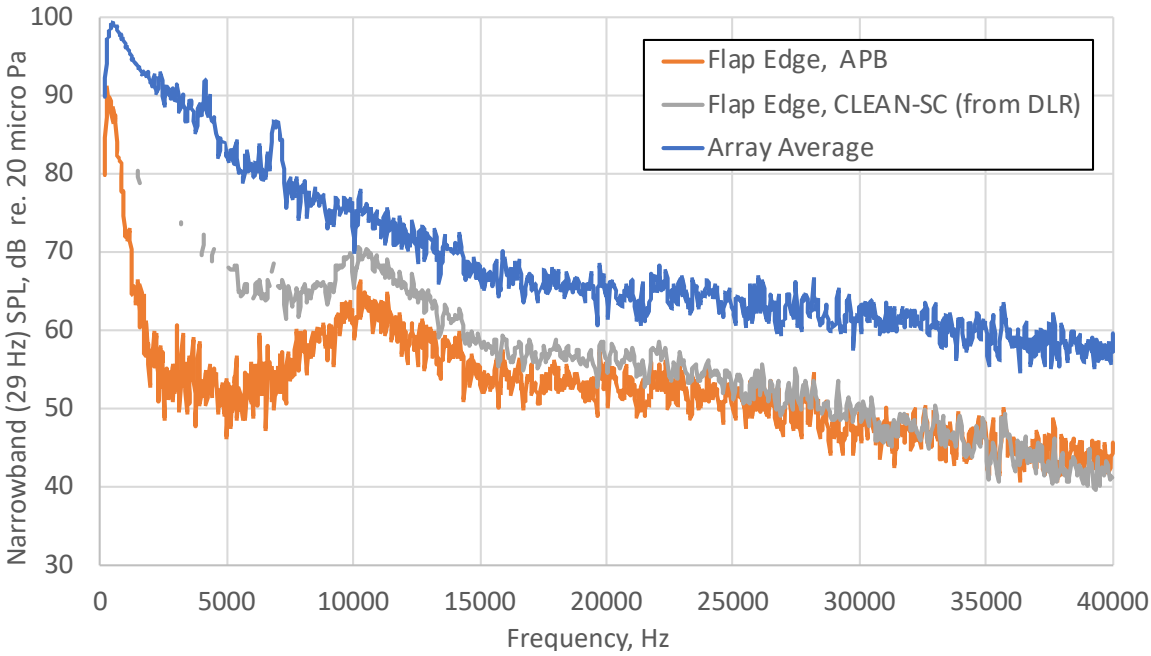

Fig. 11 Narrowband flap edge spectra for DLR 1 from APB and CLEAN-SC. The CLEAN-SC results are from Ref. 8.

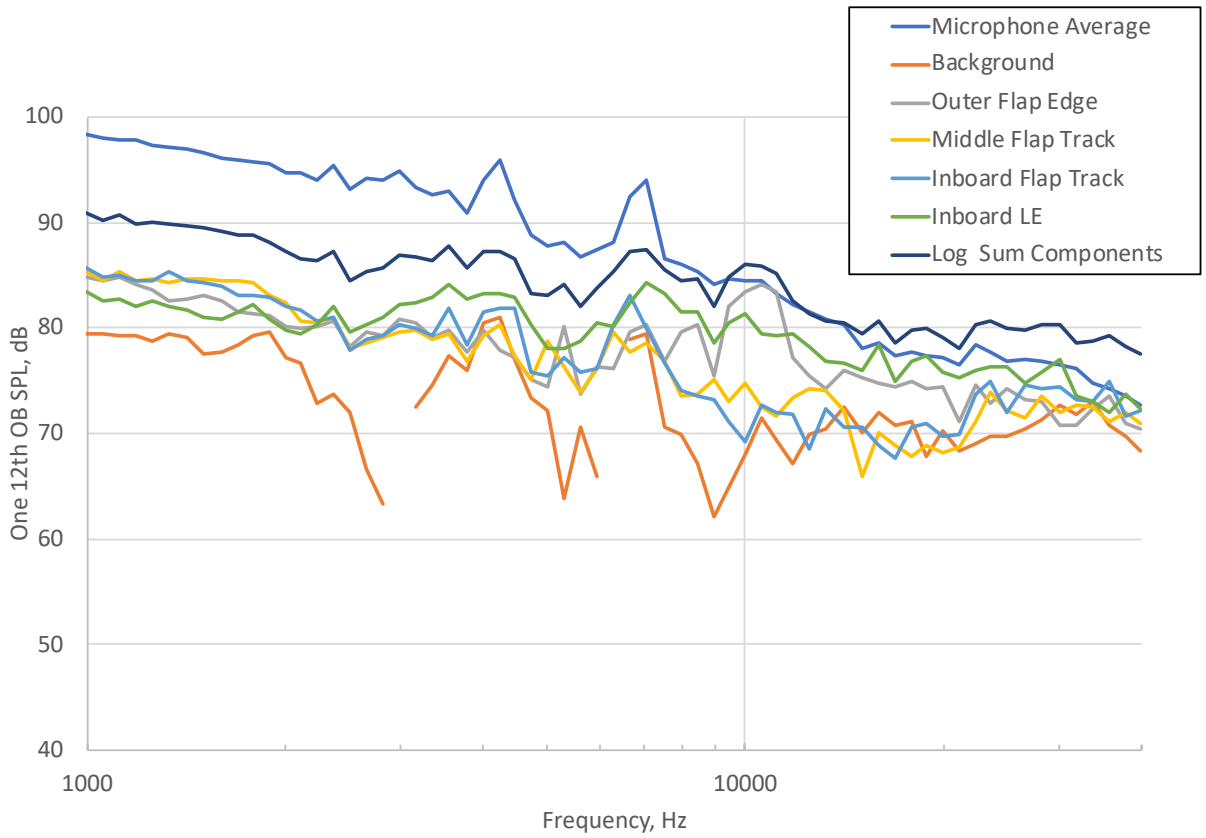

Fig. 12 Conventional beamforming integration results for the DLR 1 components.

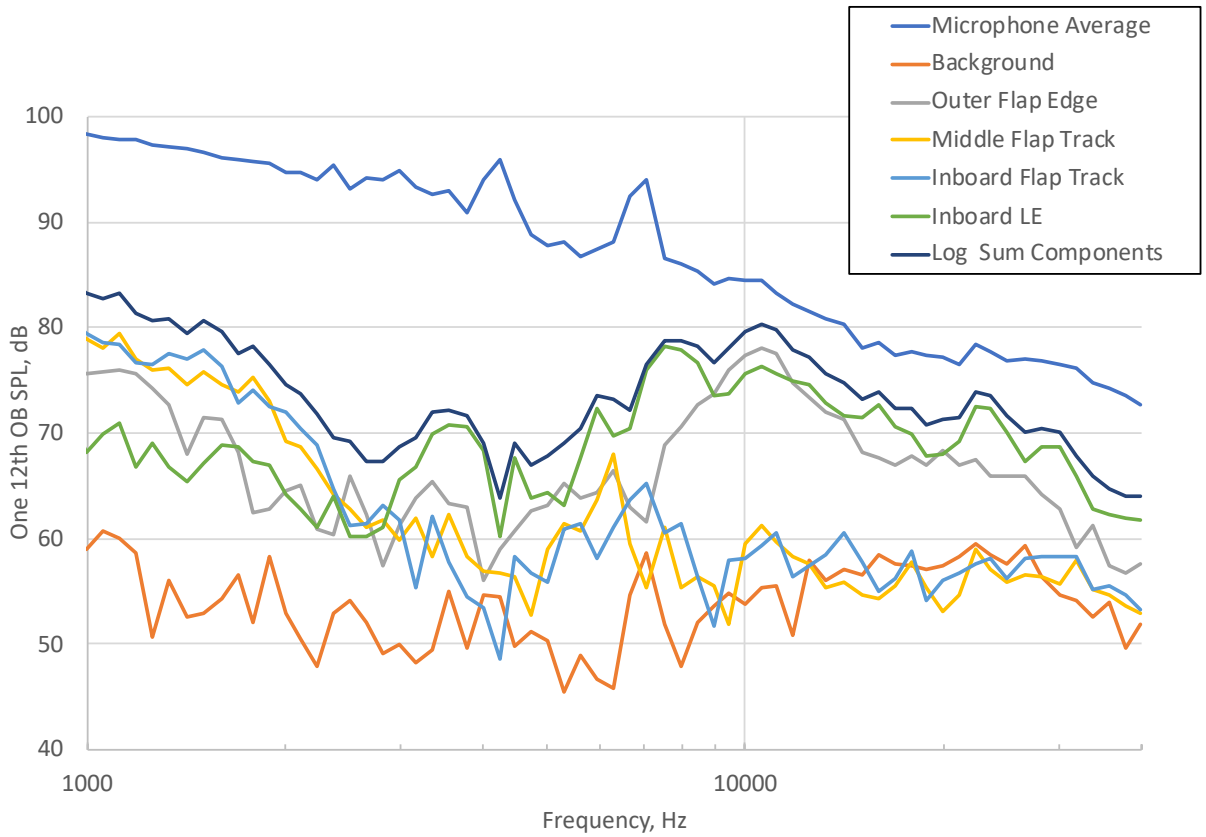

Fig. 13 Adaptive Projection Beamforming integration results for the DLR 1 components.

3.3 NASA-2

Array Methods Experimental Benchmark NASA-2 is "a NACA 63-215 full-span airfoil, with a 16-inch (0.406-meter) chord length and 36-inch (0.914-meter) span, was mounted at a -1.2 degree angle of attack to the vertical flow in the NASA Langley Quiet Flow Facility (QFF)" [9]. See also [7] and [10]. The Mach number in the QFF jet was 0.17. The first 5% of the leading edge was treated with grit to ensure a turbulent boundary at the trailing edge, but the grit provided an extra noise source at the leading edge, in addition to the main source of interest, the trailing edge noise.

Figure 14 shows the setup, including the 33-microphone Small Aperture Directional Array (SADA). The acoustic travel times for processing of the open jet configuration data were computed by assuming a broken-line ray path with an in-flow and an out-of-flow segment. The time was computed by summing the uniform-flow values for each of the two segments. The refraction point on the shear layer for each grid point/microphone pair was found by using Fermat's principle in an optimizer with two variables.

Functional Beamforming plots summed to octave bandwidth, are show in Fig. 15. Details of the LE and TE ROIS, showing some of the selected source points, and the SADA array pattern are shown in Fig. 16. The circle in the right side of Fig. 16 shows which outer microphones were excluded for frequencies above 10 kHz, so $N = 33$ for frequencies below

10 kHz and 25 above 10 kHz. The parameters for the APB were M_1 = 22, μ = 0.06, and ν = 200.

One third octave band integrated results are shown in Fig. 17. Following Refs. 7, 9, and 10, the results were scaled from the actual ROI spanwise lengths to a one-foot basis, giving dB/foot.

The model is so close to the centerline of the array that it was found to be possible to perform the beamforming using the full 1/3 octave bands in one calculation each. Calculation of two complete spectra, including the ray time optimization, took 5 seconds using one thread on a laptop computer. The full 4096 narrowbands were run as a timing test and completed in under 12 minutes using a single thread.

It can be seen the APB produces a much greater difference between the TE and LE curves than FPB does for frequencies below about 12 kHz, where the TE noise is expected to dominate.

It should be clear that the portion of the LE APB curve for frequencies below 4 kHz does not really show LE noise. It reflects the inability of the array together with the processing method to separate the LE noise from the much stronger TE noise at lower frequency.

In Fig. 18, the LE and TE APB results are superimposed on the plot from SADA processing and DAMAS processing results that was provided with the benchmark data in Ref. 9. The APB and DAMAS results compare well in this case. In overlaying the graphical results, the plot from Ref. 9 had to added second so that the APB curves would not hide many of the DAMAS symbols! Results for other methods can be seen in Figs. 9 and 10 in Ref. 7.

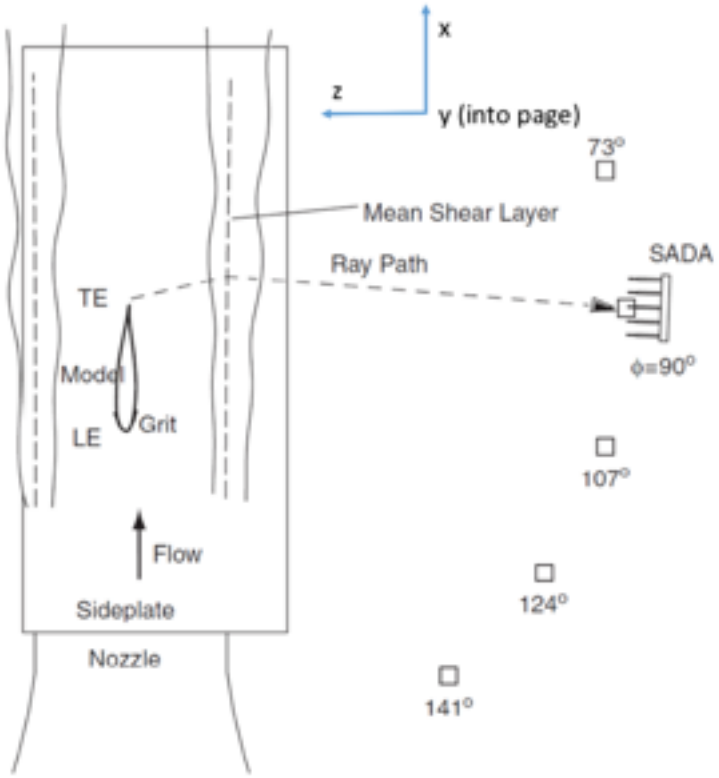

Fig. 14 Setup for the NASA-2 benchmark case. From Ref. 9.

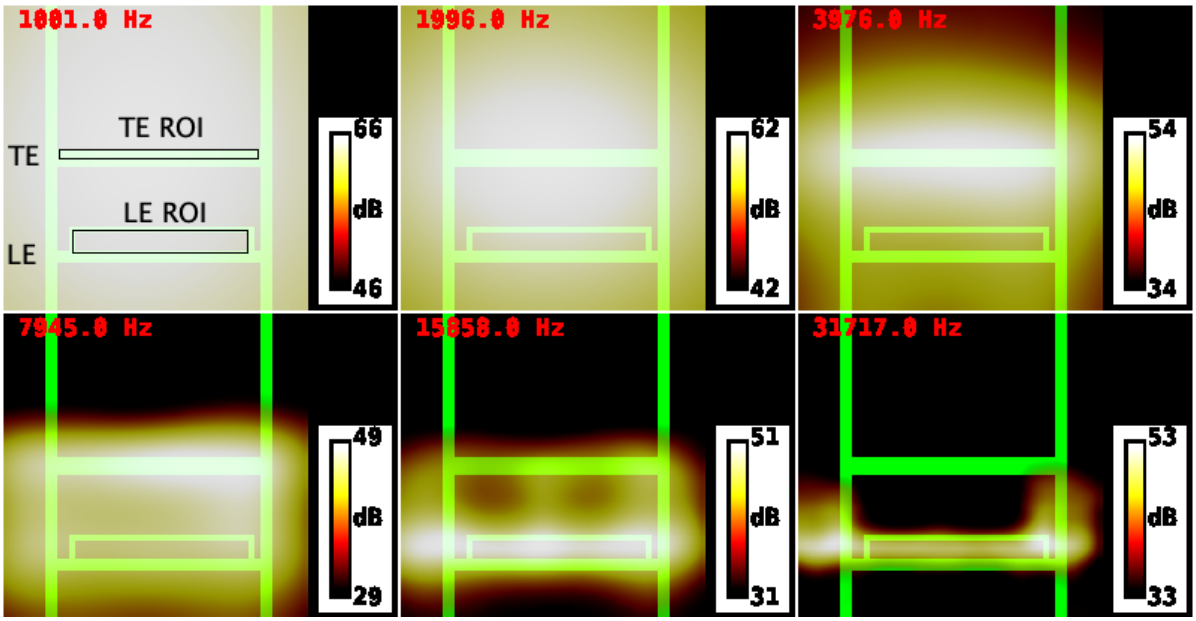

Fig. 15 Functional Beamforming results for ν = 200 for NASA-2, summed to one-octave band.

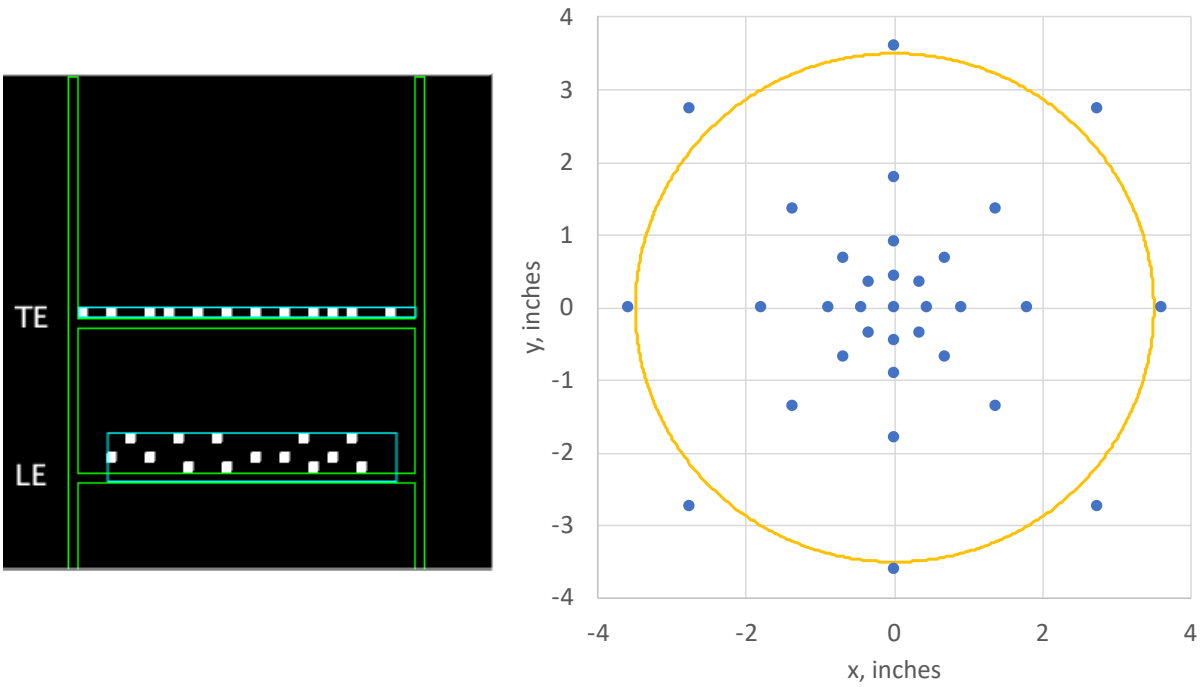

Fig. 16 Source point grid for NASA-2, left, and the pattern of the SADA array, showing the radius cutoff that was applied for 10 kHz and above.

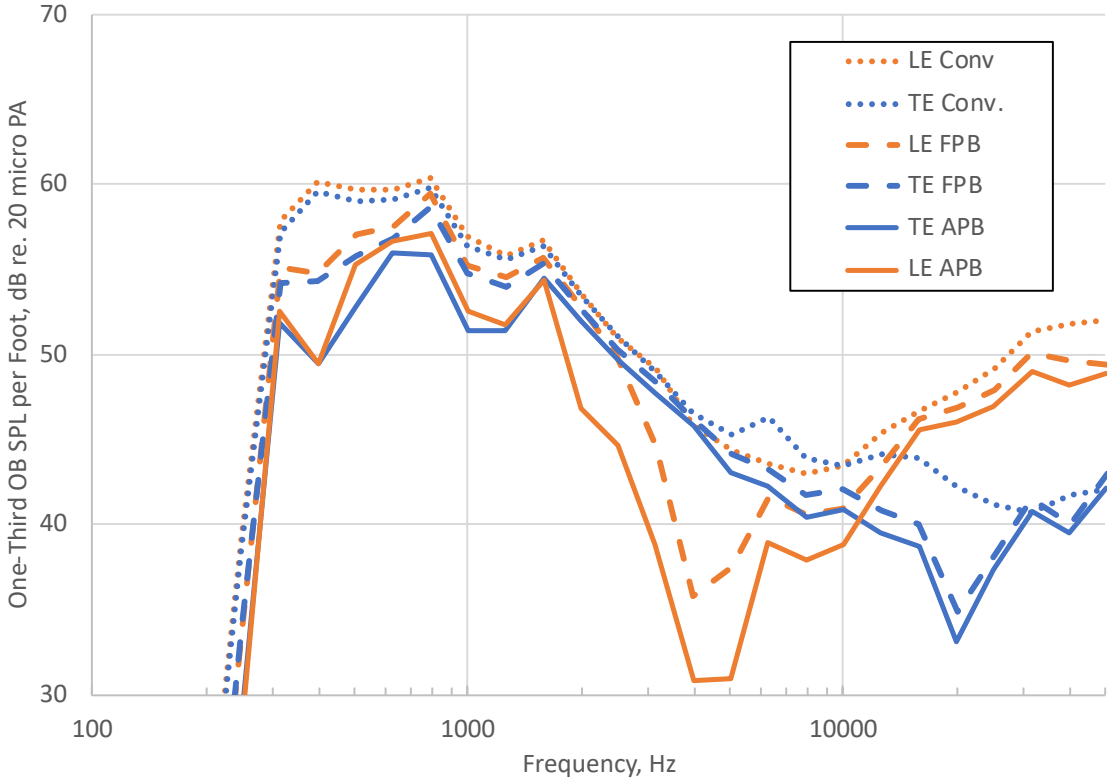

Fig. 17. LE and TE results for different integration methods for NASA-2.

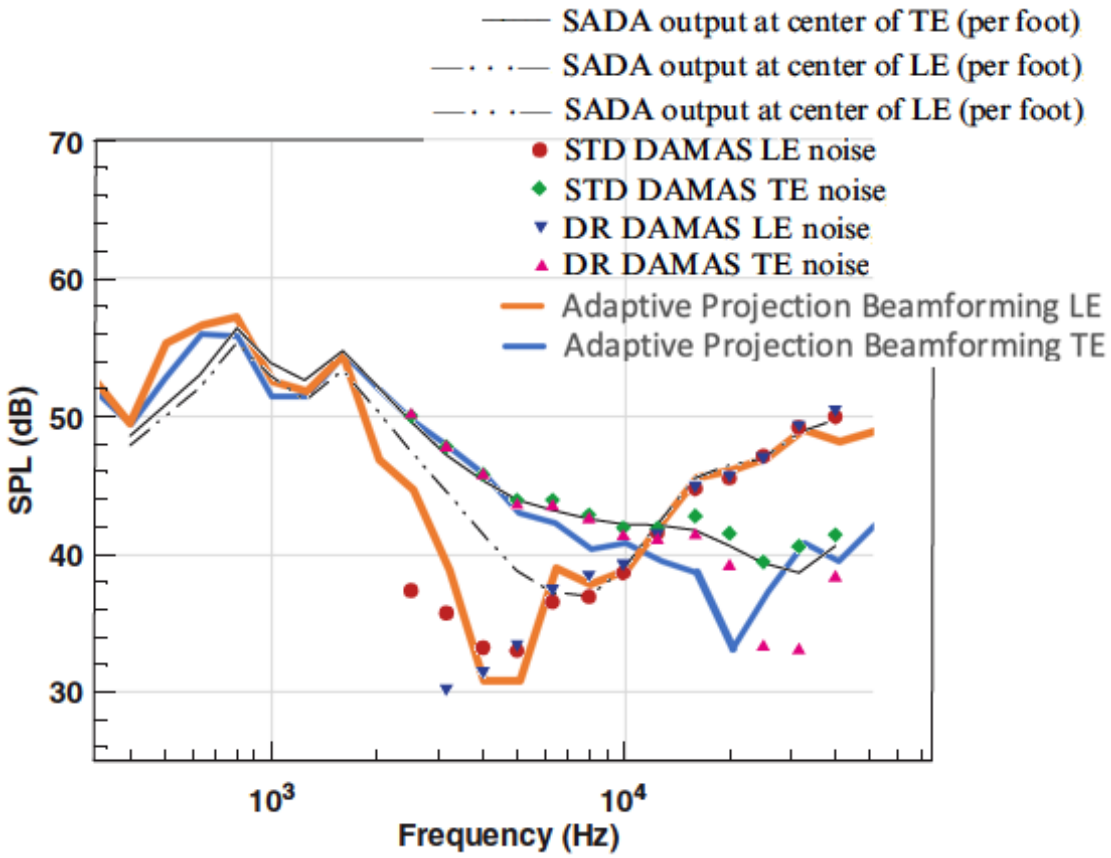

Fig. 18. Comparison of the LE and TE results from applying APB to NASA with the DAMAS and SADA output results from Ref. 9.

4 CONCLUSIONS

Adaptive Projection Beamforming (APB) improves the resolution of Functional Projection Beamforming (FPB) by a factor of about 2. Careful selection of the grid points in the Region of Interest can give good results from FPB and APB at high frequency. Applying APB to two Array Methods Experimental Benchmark test cases gave spectral results that are in line with other advanced methods. The run time of APB is much lower than deconvolution methods because only a few grid points with the Regions of Interest need to be considered. There are currently several tuning parameters in the APB method. Future work should aim for a systematic way to determine these parameters.

5 ACKNOWLEDGEMENTS

This work was supported in part by a NASA SBIR, contract number 80NSSC19C0378, technical point of contact Christopher Bahr.

Roberto Merino-Martinez proofread a draft and made a number of useful suggestions.

REFERENCES

[1] Dougherty, R.P., “Determining Spectra of Aeroacoustic Sources from Microphone Array Data” AIAA Paper 2019-2747.

[2] Merino-Martinez, R. G. Herold, M. Snellen, and R. P. Dougherty, “Assessment and comparison of the performance of functional projection beamforming for aeroacoustic measurements”, BeBeC 2020-S7.

[3] Dougherty, R.P., “Functional Beamforming”, Berlin Beamforming Conference, BeBeC 2014-1, 2014.

[4] Dougherty, R.P., "Functional Beamforming for aeroacoustic source distributions", AIAA Paper 2014-3066, 2014.

[5] Merino-Martinez, R, M. Snellen and D.G. Simmons, “Functional Beamforming Applied to Full Scale Landing Aircraft”, BeBeC-2016-D12.

[6] Dougherty, R.P, R.C. Ramachandran and G. Raman "Deconvolution of Sources in Aeroacoustic Images from Phased Microphone Arrays Using Linear Programming,", AIAA Paper 2013-2210, Berlin, Germany, 2013.

[7] Bahr, C.J., W.M. Humphreys, D. Ernst, T. Ahlefeldt, C. Spehr, Q. Leclère, C. Picard, R. Porteous, D. Moreau, J.R. Fischer, and C. Doolan, “A Comparison of Microphone Phased Array Methods Applied to the Study of Airframe Noise in Wind Tunnel Testing,” AIAA Paper 2017-3718.

[8] Ahlefeldt, T., “Array Methods HDF5-Benchmark data” Downloaded from https://www.b-tu.de/fg-akustik/cloud/ maintained by Thomas Geyer, January, 2020.

[9] Bahr, C. “Experimental Data Benchmark Problem NASA 2 (Revision 2) – Airframe Noise Test in Open Test Section”, Downloaded from https://www.b-tu.de/fg-akustik/cloud/ maintained by Thomas Geyer, January, 2020.

[10] Brooks, T.F. and W.M. Humphreys, Jr. “A Deconvolution Approach for the Mapping of Acoustic Sources (DAMAS) determined from phased microphone arrays,” AIAA Paper 2004-2954, 2004.